Supplementary Figure Legends

Figure S1. Effect of nucleotide state of MT on dimeric KIF5C motility.

MT gliding velocity of dimeric KIF5C (K375). GMPCPP-MT: 1005 ± 30 nm/s (n=50), GDP-taxol-MT: 809 ± 49 nm/s (n=50).

Figure S2. Details of the cryo-EM structures solved in this study and comparisons to the structures solved previously.

(A) Raw data image of KIF5C(Ø) bound GMPCPP-MT.

(B, C) KIF5C(Ø)-taxol-MT (B) and KIF5C(Ø)-CPP-MT (C) solved in this study were compared to KIF5B(Ø)-taxol-MT solved previously (EMDB: 5165 and 2765) (Atherton et al., 2014; Sindelar and Downing, 2007) with the difference map ($\sigma \approx 2.0$). The deposited atomic model (4UXO, orange) and KIF5(Ø)-CPP-MT pseudoatomic model (light blue) were docked in maps. Our KIF5C(Ø)-CPP-MT map and Sindelar's and Atherton's KIF5(Ø)-taxol-MT maps had differences in both kinesin and MT surface. On the other hand, no major conformational difference was seen between our KIF5(Ø)-taxol-MT and theirs. Albeit the beta-sheet densities are better separated in the Sindelar's and Atherton's maps than those in ours, the densities of α-helices of the three KIF5(Ø)-taxol-MT maps were very similar, suggesting that these structures solved by the different algorithms is very similar each other and that our maps are also generally correct.

(D) Resolutions of cryo-EM maps estimated by Gold-standard FSC function.

(E) FSC between our maps vs Sindelar's and Atherton's map. The resolution values estimated in (D) are confirmed.

(F) Local resolution calculated by ResMap. The median resolution is 8.4 Å.

(G) Cryo-EM structures of CPP-MT (Yajima et al., 2012), KIF5(Ø)-CPP-MT and KIF5(Ø)-taxol-MT. Dashed circles show the holes of intra-tubulin-dimer interfaces, and the squares show the holes of inter-tubulin-dimer interfaces. The size and shape of the holes of MTs were affected by kinesin binding, GTP hydrolysis of β-tubulin and taxol binding, suggesting that the conformational changes of tubulin were induced to alter both the longitudinal and the lateral contacts. White arrowheads indicate the major differences on the MT surface at the minus-end of α-tubulin.

Figure S3. Crystal Structure of nucleotide-free KIF5C.

(A) Electron density map around the p-loop of the KIF5C (K334) with ADP (2fo-fc, σ = 1.0). The weakly bound ADP without Mg^{2+} is observed.

(B, C) Comparisons of the nucleotide-binding pocket between the nucleotide-free KIF5C solved here and previously solved KIF5 structures, 1MKJ (B) and 2KIN(C).

(D) RMSD between nucleotide-free KIF5C solved here and other KIF5 crystal models solved previously. These comparisons suggested that our nucleotide-free structure is most similar with 2KIN in both the overall conformation and local switch I conformation. Considering that 2KIN does not possess magnesium in the nucleotide-binding pocket, the open conformation might be suitable for the ADP releasing state or the nucleotide-free state.

Figure S4. In silico docking of the atomic models into cryo-EM map of KIF5(Ø)-CPP-MT.

(A) Fitting curves of the three parameters, average map value (solid line), atoms inside

the contour (dashed line) and cross-correlation coefficient (dotted line), comparing the 1 (monomer), 2 (N/IC, NI/C and NC/I), 3 (N/I/C), and 4 (N1/N2/I/C) subdomain fittings of α-tubulin (red) and β-tubulin (blue). The 3 subdomain fitting and 4 subdomain fitting were choosed as final models for α- and β-tubulin, respectively (dark color plots).

(B) Transition of fitting parameters for one tubulin dimer through the docking trails. "Subdomain fit" means the union of 3 subdomain fitting of α-tubulin and 4 subdomain fitting of β-tubulin.

(C) The local fitting scores of the α3 and α4 before and after the subdomain fitting of the crystal structure of KIF5(Ø).

(D) Fitting curves of KIF5 from the overall-rigid body fitting to the subdomain fittings.

(E) Cross correlation values between the experimental map and a map calculated from the docked atomic models at 9 angstroms resolution. Previously solved KIF5B(Ø)-taxol-MT data was presented for comparison (Sindelar and Downing, 2007).

(F) Ten helical densities detected by Sculptor. The yellow helices correspond to the helix α4 of KIF5C and C-domain helices of α-tubulin.

(G) In-silico docking of C-domain of α-tubulin. The conformational difference before (gray) and after (red) the docking was shown. The model after the docking matches to the detected helix (yellow).

(H) In-silico docking of the switch II α4. The conformational difference before (gray) and after (green) the docking was shown. The detected α4 helix (yellow) was used as a guide.

(I) The fitted C-domains in α- and β-tubulin.

(J) Fitness of switch II seen from minus-end. A density of α4 is well resolved as a tube shape. L11 can be observed as a strong density that touches MT surface and stretches

into α4. L9 and L12 may move like the red arrows.

Figure S5. Conformations of KIF5 on MT.

(A) The left side view of the difference map between CPP-MT and KIF5(Ø)-CPP-MT at 2.0 σ. Related to Figures 5A and B.

(B) Difference map between CPP-MT and KIF5(Ø)-CPP-MT at 2.0 σ, seen from the MT minus-end at the level of β-tubulin. IC: inner contact. Related to Figures 5D and E.

(C) Schematic representation of lateral contacts between GMPCPP-MT with and without KIF5C motor.

Figure S6. Conformations of KIF5 on MT.

(A) Comparison of KIF5 structures around the nucleotide-binding pocket among two nucleotide free structures and one ADP-AlF_4 state structure that was calculated from the deposited atomic model (PDB ID: 4HNA). The switch I (α3-L9) conformation is very similar among them, albeit the loop L5 approaches closer to the nucleotide-binding pocket in KIF5C(Ø)-CPP-MT than that of the others.

(B) Previously solved cryo-EM structure of KIF5B complexed with taxol-MT (Sindelar and Downing, 2010) and docked Eg5 and KIF5 models. The helix α4 of nucleotide-free KIF5B on GDP-taxol-MT matches well to the Eg5 in the Mg-ADP state (red; PDB ID: 1II6) in preference to that in the AMPPNP state (blue; PDB ID: 3HQD) or the pseudo-atomic model of KIF5B deposited by Sindelar and Downing (green; PDB ID: 2P4N). This suggests that the nucleotide-free KIF5B on taxol-MT adopts ADP-like conformation with the long helix α4.

(C) KIF5C(Ø)-CPP-MT solved here (left), nucleotide-free Kar3 complexed with

GDP-taxol-MT (middle) and Kar3 in the AMPPNP state complexed with GDP-taxol-MT (right). Nucleotide-free Kar3 complexed with GDP-taxol-MT has a strong density corresponding to the loop L11, similar to KIF5C(Ø)-CPP-MT. This density is not observed in Kar3 in the AMPPNP state.

Figure S7. Interfaces between KIF5C and GMPCPP-MT/GDP-taxol-MT.

(A) Cross sections illustrate the interfaces of KIF5C in KIF5(Ø)-CPP-MT (left) and KIF5(Ø)-taxol-MT (right).

(B) Elements that contribute to the KIF5C-MT interaction. Left panel shows the MT-interacting elements of KIF5C seen from the MT-binding side. Right panel shows the KIF5C-interacting elements of MT seen from the MT-surface. Blue, KIF5(Ø)-CPP-MT; yellow, KIF5(Ø)-taxol-MT. The table below shows a summary of the interacting elements.

Movie S1. Cryo-EM structure of KIF5(Ø)-CPP-MT and atomic models before and after the subdomain docking. Cryo-EM map is depicted in two different contour levels at 1.5 and 1.8 σ. Pink, N- and I-domains of α-tubulin; magenta, C-domain of α-tubulin; light blue, N- and I-domains of β-tubulin; navy, C-domain of β-tubulin; cyan, KIF5C(Ø); greenish yellow, switch I; yellow, switch II. White loops (L8,9,12, NIS) may possibly move.

References

Atherton J, Farabella I, Yu IM, Rosenfeld SS, Houdusse A, Topf M, Moores CA (2014) Conserved mechanisms of microtubule-stimulated ADP release, ATP binding, and force generation in transport kinesins. *Elife* **3**

Sindelar CV, Downing KH (2007) The beginning of kinesin's force-generating cycle visualized at 9-A resolution. *J Cell Biol* **177:** 377-385

Sindelar CV, Downing KH (2010) An atomic-level mechanism for activation of the kinesin molecular motors. *Proc Natl Acad Sci U S A* **107:** 4111-4116

Yajima H, Ogura T, Nitta R, Okada Y, Sato C, Hirokawa N (2012) Conformational changes in tubulin in GMPCPP and GDP-taxol microtubules observed by cryoelectron microscopy. *J Cell Biol* **198:** 315-322

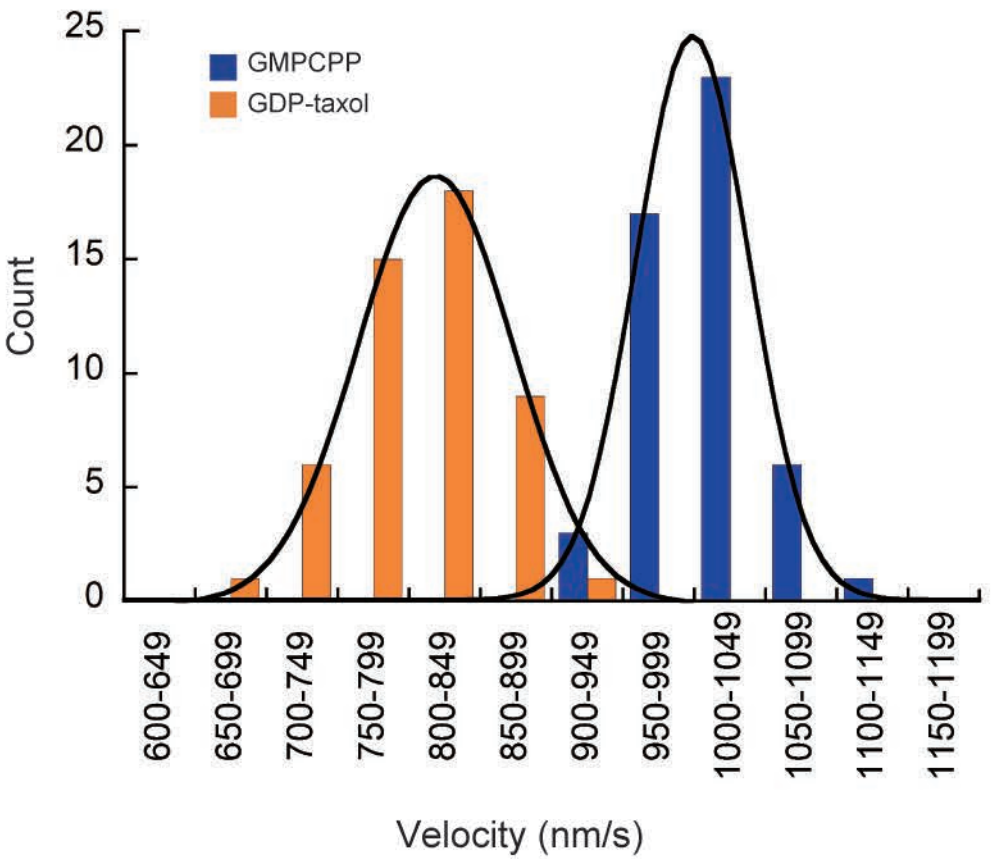

Fig.S1 Morikawa et al.

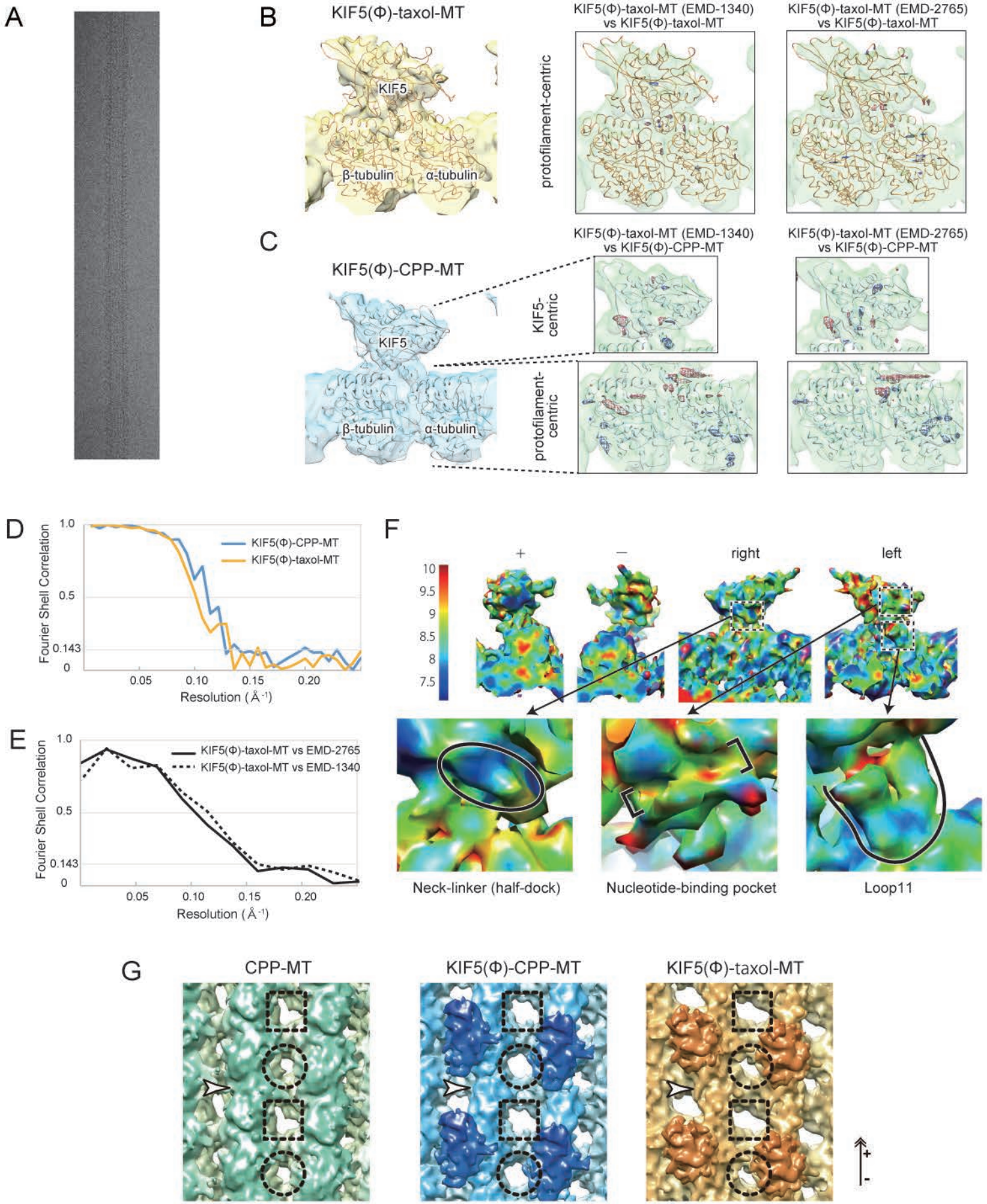

Fig.S2 Morikawa et al.

A

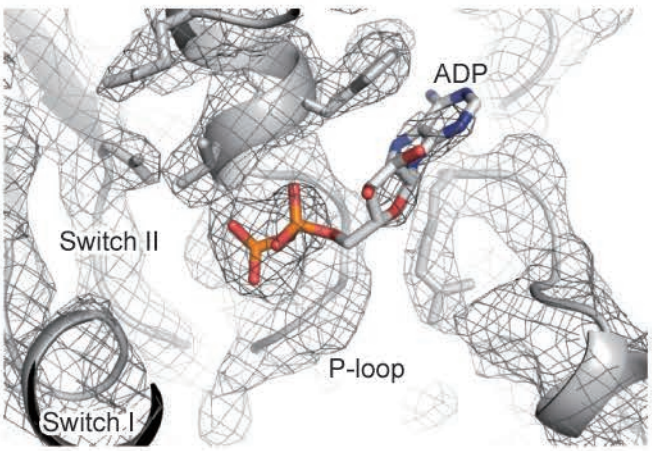

B

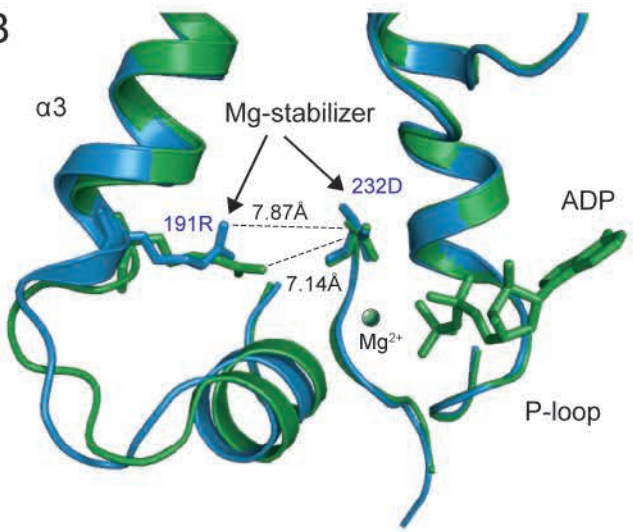

C

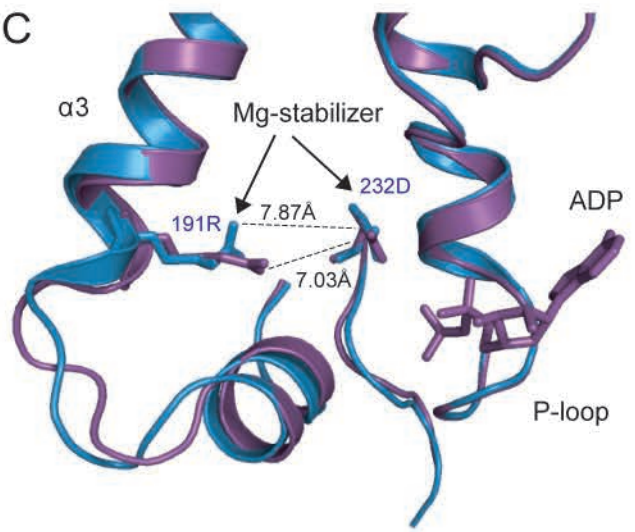

D

Table 2. RMSD between nucleotide-free KIF5C and other KIF5 models.

PDB ID	overall (Å)	α3 (Å)
1BG2	1.344	1.070
4HNA	1.051	1.164
1MKJ	0.789	0.835
2KIN	0.739	0.610

Fig.S3 Morikawa et al.

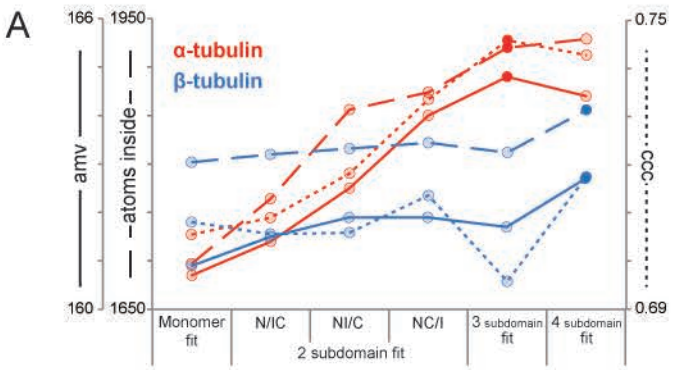

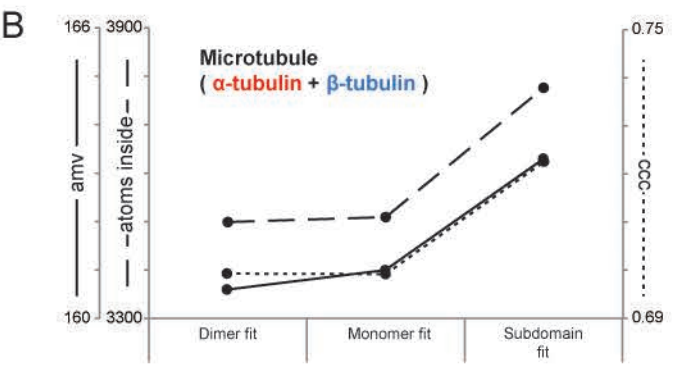

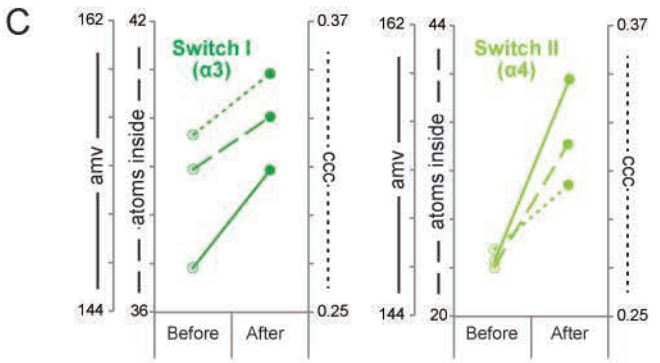

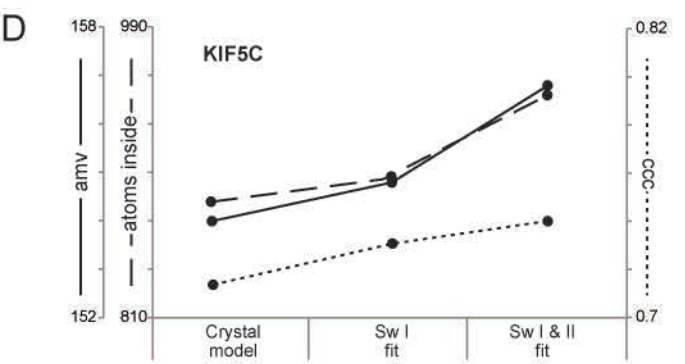

E

Table 3. Cross correlation with 9 Å simulated map

KIF5(Φ)-CPP-MT vs docked model	KIF5(Φ)-taxol-MT (EMD-1340) vs 2P4N
93.5	90.8

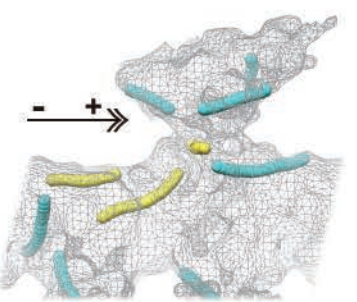

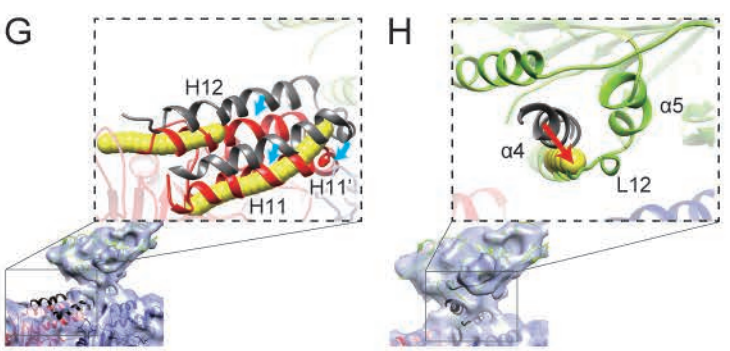

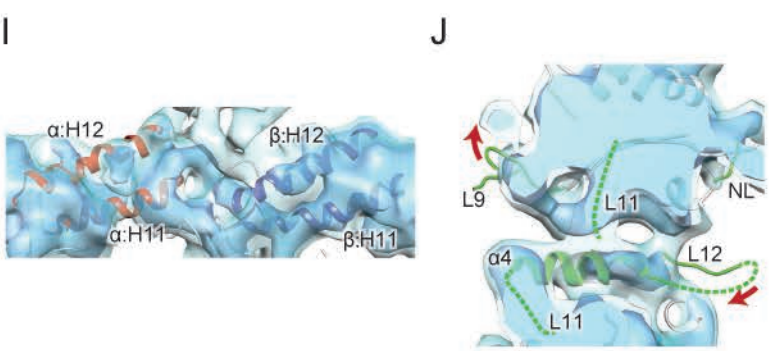

Fig.S4 Morikawa et al.

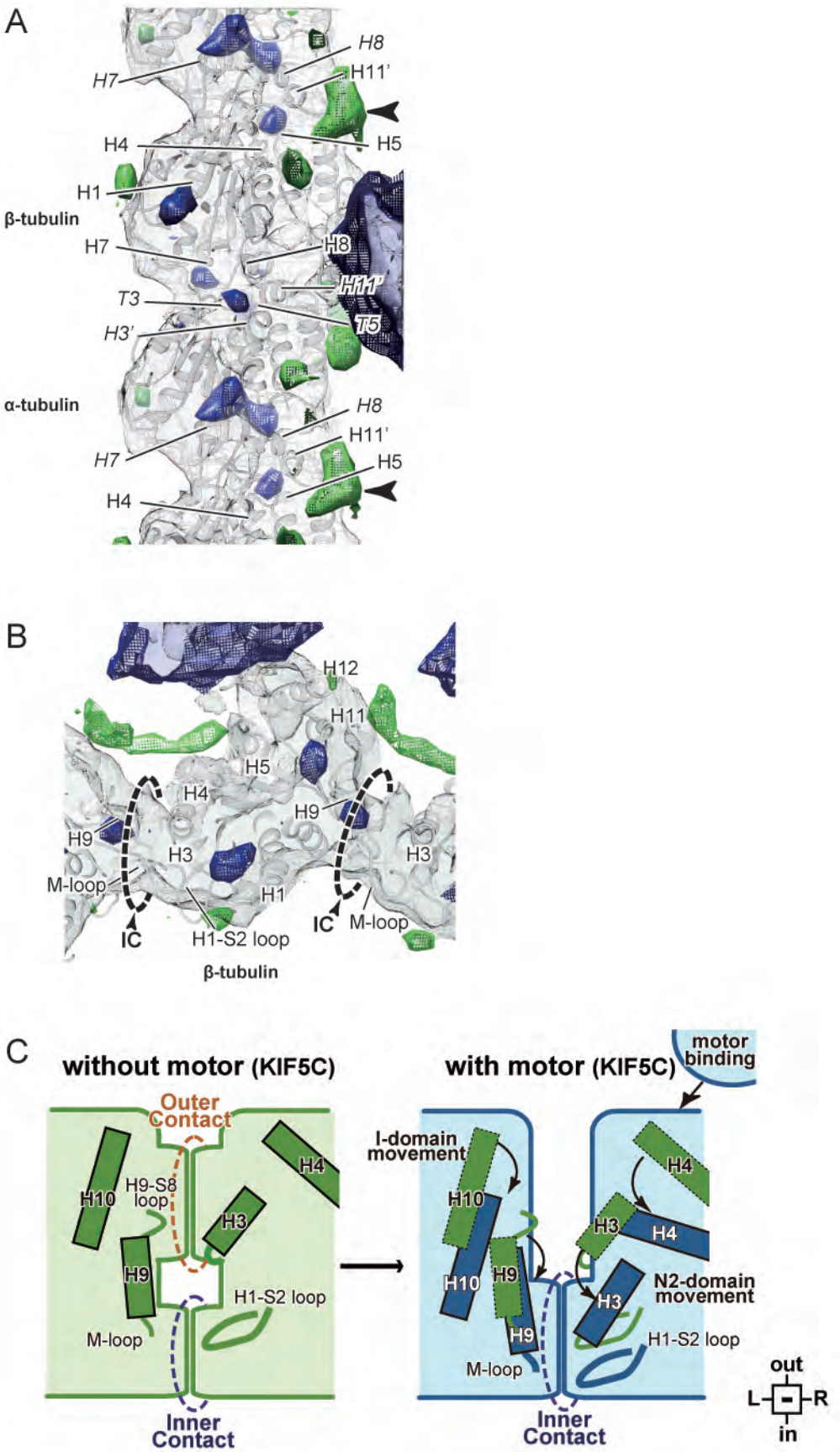

Fig.S5 Morikawa et al.

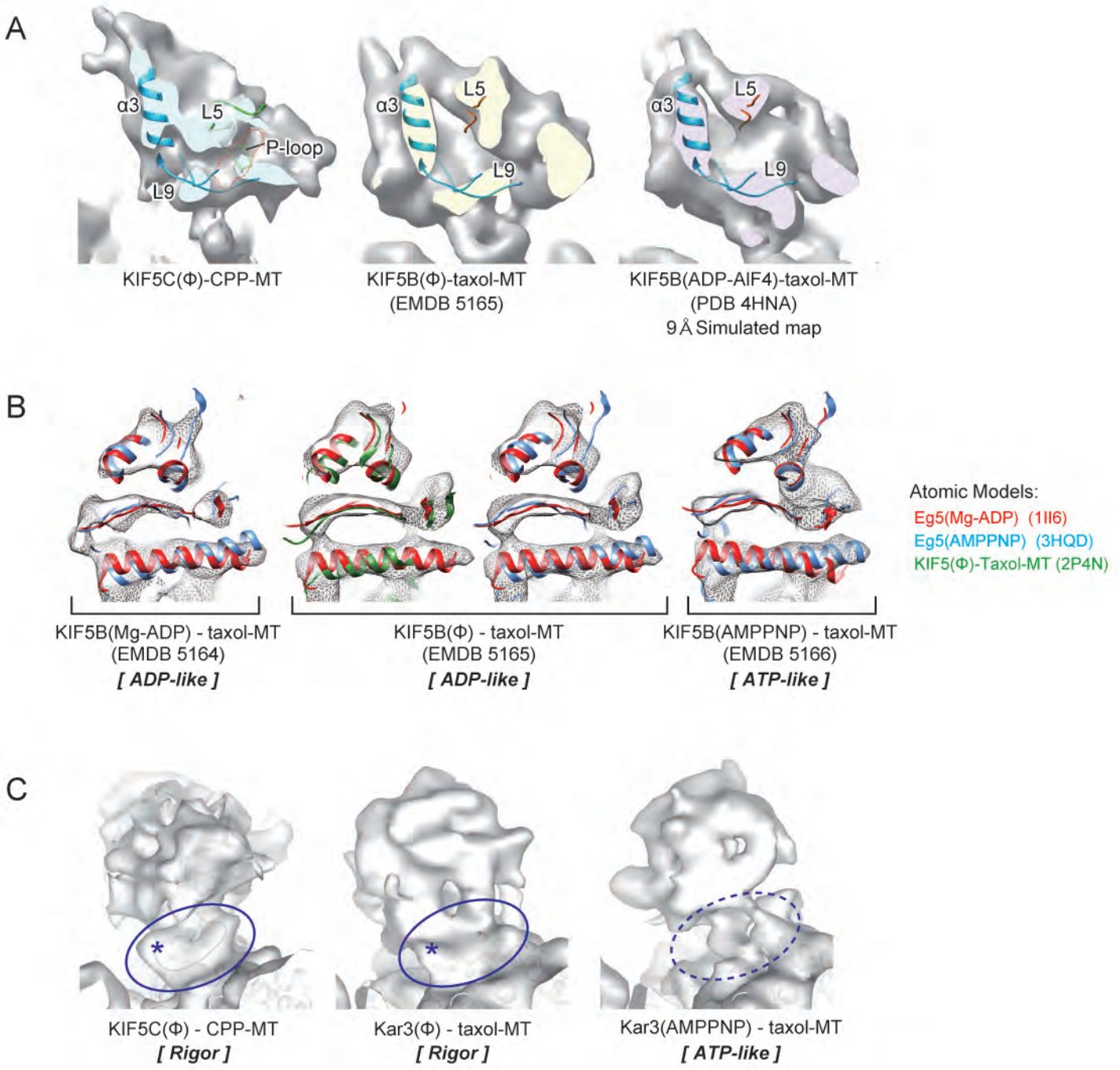

Fig.S6 Morikawa et al.

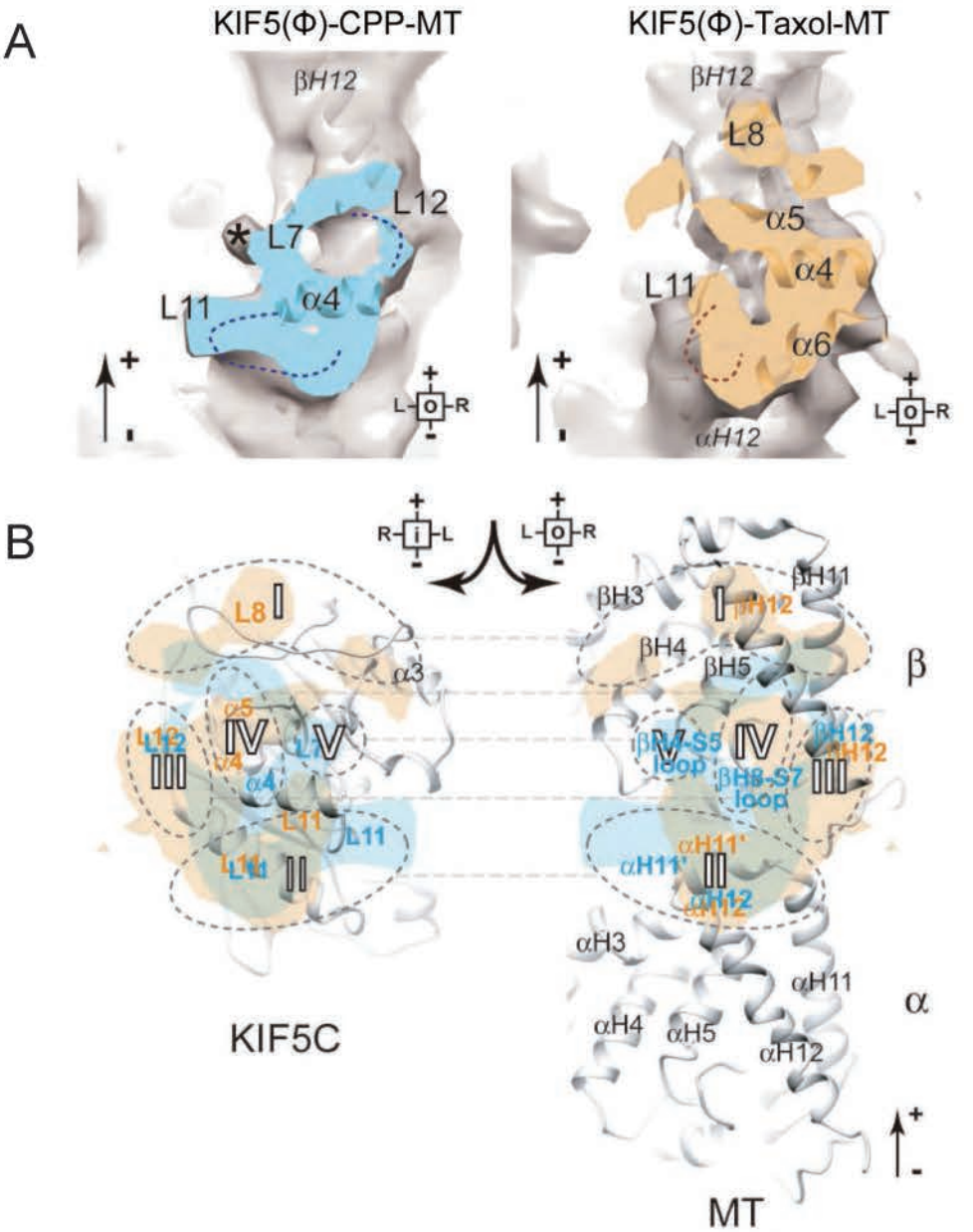

contact component	KIF5C	GMPCPP-MT	KIF5C	GDP-taxol-MT
I (plus end)		weak	L8	βH12 (N)
II (minus end)	L11	αH12(N)-H11'(C)	L11	αH12(N), H11'
III (right)	L12	βH12 (C)	L12	βH12 (C)
IV (center)	α4	βH4-S5 or βH8-S7 loop	α4, α5	βH12
V (left)	L7	βH4-S5 or βH8-S7 loop		(-)

Fig.S7 Morikawa et al.